Collective Behaviour in suspensions of pushers and pullers

Master Thesis
in
Biophysical Chemistry

Performed at
Division of Physical Chemistry,
Department of Chemistry
Lund University

By
Shan Anjum

Supervisor Joakim Stenhammar
Co-Supervisor Dora Bardfalvy
Examiner Kristofer Modig

Lund University

June 11, 2019

Teknisk Nanovetenskap, Lunds Tekniska Högskola,
Lunds universitet

Engineering Nanoscience, Credits, Faculty of Engineering,
Lund University

Abstract

Microswimmer is a term that denotes small selfpropelling agents, such as bacteria, algea or artificial robots. Depending on the flow field they set up they can be categorized into two classes *pushers* (e.g. *E. coli*) and *pullers* (e.g *C. reinhardtii*). The occurrence of jets, eddies and flocking have been observed in systems of dens pusher suspension. This phenomenon is called active turbulence. The transition to active turbulence has been attributed to hydrodynamic interactions reorienting and aligning pushers, whereas the same type of hydrodynamic interactions destroy collective motion in puller suspensions. This thesis sets out to investigate the properties of active turbulence in mixtures of pushers *and* pullers by means of particle-based Lattice Boltzmann simulations. Two body interactions between microswimmers and properteis regarding fluid statistics and swimmer statistics in 3-dimensional suspensions were investigated. Similar studies were also performed on a class of nonswimming particles, so called shakers. Our results shows that the presence of pullers in a pusher suspension can inhibit active turbulence. Furthermore we have observed that a suspension consisting equal parts pullers and pushers will display properties similar to a noninteracting system.

Preface

This is the report for my 30 credit degree project in biophysical chemistry performed at the division of Physical Chemistry, Faculty of Science, at Lund university. The project was commenced in February of 2019 and completed in june 2019. The thesis is the concluding assignment of a Master of Science Degree in Engineering Nanoscience at LTH, the Faculty of Engineering of Lund University.

I would like to express my appreciation and thank my supervisors Joakim Stenhammar and Dora Bárdfalvy for their patience, support and physical insight. Without them this thesis would not be. I would also like to thank Dora in her role as office mate, your company was comforting and talking to you about cats was fun. I wish also to express my gratitude to Linnea, Tommy and Erika for making the coffe breaks extra fun, catching up with you was always exciting. The encouragement and support from my family and friends has been invaluable during this process. I express my gratitudes towards my mother for always caring and my father for supporting me, i would like to thank my sister Sarah and my cousin Ali for always being there for me, without your support, encouragement and love i would not be where i am today.

Populärvetenskaplig sammanfattning

Bakterier som lever i vatten brukar ta sig fram med hjälp av långa trådliknande utskott, så kallade flageller. Denna simteknik är väldigt annourlunda jämfört med det vi oftast ser i vår omvärld, att simma med fenor eller åror är nämligen inte särskilt effektivt för bakterier. Detta har att göra med vattnets radikalt annourlunda hydrodynamiska egenskaper på mikroskalan. Man brukar tala om det så kallade Reynoldstalet, Re, det sammanfattar hur tröghetskrafter och friktionskrafter på en fast kropp i en vätska jämför sig gentemot varandra. Då vi människor brukar simma upplever vi höga Reynoldstal ($Re \sim 10^6$). Detta innebär att tröghetskrafterna dominerar, och förklarar varför man kan fortsätta glida en bra bit efter att man tagit ett rejält simtag. För en *E. coli* bakterie, brukar friktionskrafterna dominera. Då den slutar rotera med flaggelerna så stannar den omedelbart ($Re \sim 10^{-5}$). För en människa skulle detta motsvara att simma i honung. Bakterier och andra mikroorganismer har därför utvecklat andra, mer effektiva simtekniker.

Det kan förefalla opraktiskt att leva i en sådan högviskös värld; dock leder de hyrdodynamiska egensakperna till väldigt exotiska och spännande fenomen. Ett av de mest utforskade fenomen har observerats i koncenterade bakteriesuspensioner av *E .coli* och *Sallmonella*. Vid volymkoncentrationer större än 2 procent har man observerat att bakterierna slutar simma på ett oorganiserat sätt och börjar då istället bilda "flockar". Flockarna rör sig på ett koordinerat sätt på långa längskalor med hastigheter mycket större än de indivudella simmarnas. Bakteriernas simmmande ger även upphov till kaotiska flödesmönster väldigt lika turbulens. "Klassisk" turbulens, som man t.ex kan observera kring en flygplansvinge, brukar dock ske för höga Reynoldstal ($Re > 1000$). Detta fenomen, kallat *bakteriell turbulens*, sker vi betydligt lägre Reynolds tal och har därför en annan underliggande mekanism.

Då en bakterie simmar ger den upphov till ett flödesfält. Bakterier i närheten av flödesfältet kommer då att orienteras i flödet så att de börjar simma i samma riktning. Det är detta som ger ger upphov till bakteriell turbulens. Bakteriell turbulens uppstår dock inte i alla typer av mikroorganism-suspensioner. I koncenterade suspensioner av den encelliga algen *C. reinhardtii* går det inte att observera bakteriell turbulens. Flödesfältet som *C. reinhardtii* genrerar är nämligen annourlunda än det som går att observera hos t.ex *E. coli* och kan inte ge upphov till bakteriell turbluens.

I det här examensarbetet studeras egenskaper hos suspensioner bestånde av blandningar av flödesfält som genrerar aktiv turblens, så kallade pushers, och de som inte gör det, så kallde pullers. Vi har gjort dessa studier i form utav numeriska beräkningar och datorsimulationer. Vi försöker först med att förstå oss på tvåkroppsinteraktionen mellan par av pushers, pullers och blandade pusher/puller par. Vi studerar även beteendet av flocking och den omgivande vätskans egenskaper för olika koncentrationer och bladningar av pushers och pullers. Slutligen studerar vi även egenskaper hos ickesimmande pushers respektive pullers, så kallde shakers.

Våra resultat visar att närvaron av pullers i en pusher suspension kan ha en destruktiv effekt på bakteriell turbulens. Blandningsfraktionen av pullers och pushers påverkar många egenskaper gällande den bakteriella turbulensens hydrodynamiska egenskaper. Vi har även observerat att suspensioner bestånde av lika många pushers som pullers uppvisar liknande egenskaper som icke-växelverkande suspensioner. Dessa resultt kan komma till använding då det kommer till att förstå processer där bakterier och andra mikroorganismer är relevanta. Då de nästan alltid existerar i kolonier och utgör en grundstomme i många ekologiska och biologiska processer är det lätt att tänka sig att våra resultat kan komma till använding i många olika studier. Baktierer är t.ex viktiga i kolets kretslopp, syrets kretslopp, matsmältningprocessen och infektionsförlopp. Våra resultat kan även generaliserar till artificiella mikropskopiska robotar, s.k.*"artificial microswimmers"*. I framtiden kommer man kanske kunna använda dessa för drug delivery, kirurgi och i mikrofludiska applikationer.

Contents

Chapter 1

Introduction

Most people are familiar with microorganisms in some way. We know that they are responsible for a lot of our illnesses and colds but we rarely reflect on how peculiar these small things are. From the archea in the depths of the oceans to the bacteria inside our bodies; these creatures exist in every part of the biospehre. They also play a central role in many biological and ecological processes in nature, such as digestion, reproduction, infection and CO_2 capture and mixing in the oceans [17]. Since they rarely live alone, and often exist in colonies. A thorough understanding of the collective dynamics of these microorganisms is needed when it comes modelling the aforementioned phenomena. This thesis concerns itself with the study of collective motion of selfpropelling agents,so called microswimmers. This is a term that both encompasses biological microorganism and artificial inanimate microrobots. We will start this chapter with a general introduction to swimming at the microscale. Motility and swimming mechanisms in bacteria and other microswimmers will be explored. We then move on to discuss some of the physical aspects surrounding microscale selfpropulsion. In the last section we will discuss a collective motion phenomenon, called active turbulence

1.1 Swimming at the micro-scale

Locomotion is a fundamental ability of many microorganisms such as bacteria, algae and protozoa. Without it they would not be able to collect nutrients, orient themselves toward light, spread their off-spring and form new colonies [6]. In this section we will briefly study some of these swimming techniques before reviewing the physical aspects behind them. Bacteria like *E. coli* and *S. typhimurium* propel themselves by using bacterial flagella [6, 12]. The flagellum consists of a filament, a rotary motor and a hook that connects them. The filament traces out a helix with a contour length $\sim 10\,\mu m$, the helix is left handed with a pitch of $\sim 2.5\,\mu m$ and helical diameter of $\sim 0.5\,\mu m$. Each bacterium usually has several flagella, and by turning the motor counter-clockwise the filaments wrap into a bundle that propels the organism at speeds of 20-60 µm/s [12]. If one or more of the motors start to rotate in the opposite direction, the corresponding filaments leave the bundle and a transformation takes places in which the handedness of all helix changes; this

changes the swimming direction of the bacteria, a so called tumble. This gives the bacteria a distinct kind of run-and-tumble motion with straight runs punctuated by discrete reorientations [6].

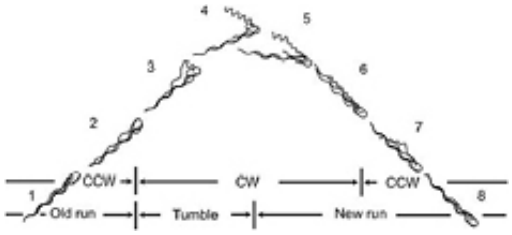

Figure 1.1: An illustration depicting a typical run-and-tumble motion. When the flagellum turn counterclockwise (CCW) they wrap up into a bundle and the bacterium performs a run. When one or more of the flagella start turning clockwise (CW) the bacteria tumbles and changes direction, in which it performs another run. Image reproduced from Ref.[6].

Eukaryotes also possess flagella, however their structure is more complex and they are usually much longer. The most common structure of eukaryotic flagella has two microtubles running along the length of the flagellum and several doublets of microtubules spaced around it, with the help of molecular motors like dynein the doublets can be slid along the axis of the flagellum, leading to bending and deformation that propagate along the flagellum. *C. reinhardtii* is a singel-cell alga that swims with two flagella, it moves by performing breast-strokes: the flagella are pulled back in a stiff and straight shape, to later be bent and pushed forward [6]. Propulsion can also occur through other means

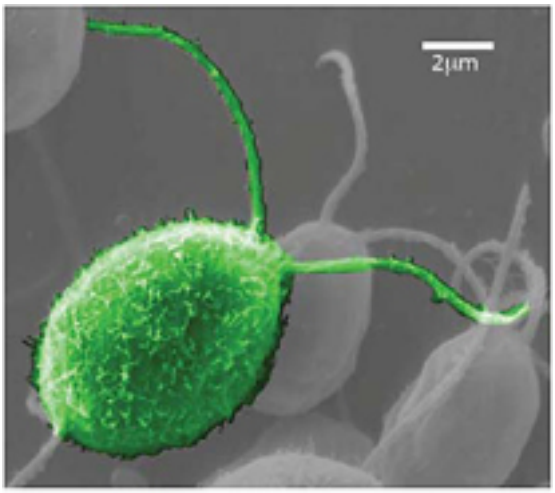

Figure 1.2: A scanning electron microscope image of *C. reinhardtii*, adapted from http://http//remf.dartmouth.edu/images/algaeSEM

.

than by using flagella. Pathogens of the genus *Listeria* can for instance hijack the actin production of host cells and use it to propel itself, while ciliates use densely packed, small appendages, called cilia, distributed over the membrane surface to move themselves [12, 6]. A thorough account of all these different propulsion techniques is not possible within the frames of this work. All microswimmers are not of biological origin, there also exists numerous artificial microswimmers [12].

A way of creating an artificial microswimmers is by using Janus particles. These are a class of particles that consists of two different halves, by giving the halves different properties selfpropulsion might be achived. One might for instances make one half catalytically active and the other passive, this gives rise to an asymmetry and a non-equilibrium distribution of reactants around the particles surface. The concentration gradient will lead to osmotic forces, which propels the particle. Propulsion does not necessarily need to rely on catalysis, laser induced heating or light might also induce propulsion [9, 4].

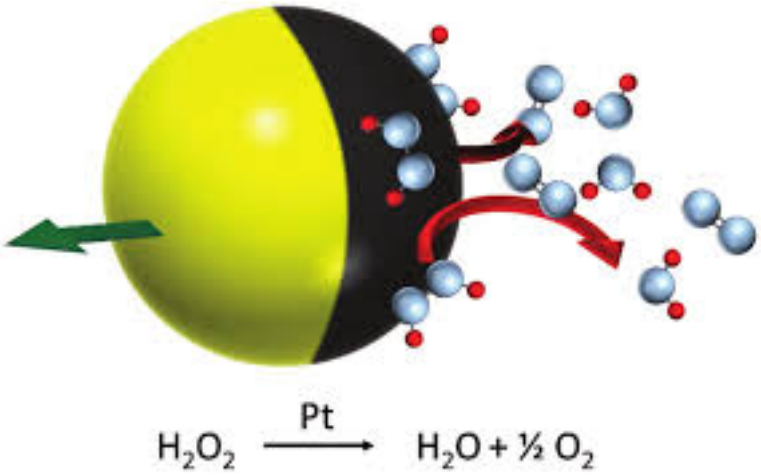

Figure 1.3: A figure depicting a catalytic Janus particle. The particles propels itself by catalysing H_2O_2 using Platinum. Image adapted from Ref.[1]

1.2 Physical aspects of swimming

In the previous section we discussed some different swimming strategies that has been utilised in nature and by synthetic swimmers. We will now look closer at some of the physical aspects of swimming on the microscale.

Forces and torques applied by the swimmer will create a flow field, described by the Navier-Stokes equation (NSE).

$$\rho(\frac{\partial}{\partial t} + \mathbf{u} \cdot \nabla)\mathbf{u} = \mathbf{F} - \nabla p + \mu \nabla^2 \mathbf{u}, \tag{1.1}$$

where $\mathbf{u}$ is the fluid velocity, ρ is density, $\mathbf{F}$ is force, p is pressure and μ is dynamic viscosity. Depending on the fluid and the circumstances one models it under, one can assume that fluid is incompressible, i.e. $\nabla \cdot \mathbf{u} = 0$, which is a suitable approximation for us, given that we will be modelling a homogeneous newtonian fluid. NSE is a nonlinear partial differential equation and only few problems can be solved analytically [12]. However at the microscale fluids behave differently compared to what we are used to. In order to proceed we need to discus the Reynolds number. The Reynolds number is a dimensionless number :

$$Re \equiv \rho U L/\mu, \tag{1.2}$$

where U and L are characteristic velocities respectively lengths. The Reynolds number can be interpreted as the the ratio between the inertial and the viscous terms in the NSE [12, 6, 8]. A bacterium for instance is typically around $L \sim 1\,\mu\text{m}$ in size. We might estimate the characteristic velocity to be $U \sim 30\,\mu\text{m/s}$ and assuming it moves in water we get $\mu \sim 1$ Centipoise [15]. The Reynolds number then becomes $Re = 3 \times 10^{-5}$. Microswimmers thus live in a world dominated by viscous forces [15]. A common approximation is therefore to take the limit $Re \longrightarrow 0$. This reduces the NSE into the Stokes equation [12, 8]:

$$\mu \nabla^2 \mathbf{u} - \nabla p = \mathbf{F}, \tag{1.3}$$

Stokes equation exhibits the following properties [8] :

1. Linearity
2. Reversibility
3. Time independence

The linearity and time-independence give rise to kinematic reversibility. Given a fluid field for a solid body moving at speed $\mathbf{U}$ and with rotation rate $\mathbf{\Omega}$ one can transform $\mathbf{U} \longrightarrow \alpha\mathbf{U}$ and $\mathbf{\Omega} \longrightarrow \alpha\mathbf{\Omega}$. Due to linearity, the velocity and pressure field transform as $\mathbf{u} \longrightarrow \alpha\mathbf{u}$ and $p \longrightarrow \alpha p$. Applying the principle of kinematic reversibility to low Reynolds number locomotion leads to two important results. The first result is that of rate independence. If a swimmer deforms its surface, the distance travelled by the swimmer between two different surface configurations does

not depend on the rate of deformation, it only dependence on its geometry, i.e the sequence of shapes the surface deforms to between these configurations. The second result is the so called scallop theorem. It states that swimming only can occur for non-reciprocal swimming strokes, i.e for swimming strokes that look different when viewed forward and backwards in time. This implies that bodies with a single degree of freedom cannot swim as they deform in a reciprocal manner [12].

Due to the linearity of the Stokes equation traditional mathematical methods based upon superposition of solutions, such as Green's function methods, can be used to solve for velocity and pressure fields [12, 30]. The fundamental solution, i.e. the Greens's function for the fluid flow for a Dirac-delta point force $\delta(\mathbf{x}-\mathbf{x}')\mathbf{F}$ is given by :

$$\mathbf{u}(\mathbf{x}) = \mathbf{G}(\mathbf{x}-\mathbf{x}')\cdot\mathbf{F}, \tag{1.4}$$

where

$$\mathbf{G}(\mathbf{r}) = \frac{1}{8\pi\mu}(\frac{\mathbf{1}}{r} + \frac{\mathbf{r}\otimes\mathbf{r}}{r^3}), \tag{1.5}$$

Where $\mathbf{G}$ is the so called Oseen tensor and $r = |\mathbf{r}|$. The flow field described by Eq. 1.4 is called a stokslet. A thorough derivation of the fundamental solution is provided in [8]. To calculate the fluid flow due to swimming one usually has to take swimming gait and geometry into account, giving us a result that varies from swimmer to swimmer. However, due to the linearity of the Stokes equation, one can also perform a multipole expansion, where the velocity field is expressed as a power series in r^{-1}. For microswimmers it generally applies that the velocity field decays as r^{-2} [30]. This is because microswimmers produce their own driving, so that there is no net external force or torque acting on the swimmer (assuming that the swimmer is neutrally buoyant). Given a force distribution $\mathbf{f}(\boldsymbol{\xi})$ we have that:

$$u_i(\mathbf{r}) = \int G_{ij}(\mathbf{r}-\boldsymbol{\xi})f_j(\boldsymbol{\xi})d\boldsymbol{\xi}, \tag{1.6}$$

By Taylor expanding about the origin we get

$$u_i(\mathbf{r}) = \int \left\{ G_{ij}(\mathbf{r}) - \frac{\partial G_{ij}(\mathbf{r})}{\partial \xi_k}\xi_k + \frac{1}{2}\frac{\partial^2 G_{ij}(\mathbf{r})}{\partial\xi_k\partial\xi_l}\xi_k\xi_l + ... \right\} f_j(\boldsymbol{\xi})d\boldsymbol{\xi}$$

By simplifying and rearranging the expression we get the following expression :

$$u_i(\mathbf{r}) = G_{ij}(\mathbf{r})\int f_j(\boldsymbol{\xi})d\boldsymbol{\xi} - \frac{\partial G_{ij}(\mathbf{r})}{\partial\xi_k}\xi_k\int \xi_k f_j(\boldsymbol{\xi})d\boldsymbol{\xi} + \frac{1}{2}\frac{\partial^2 G_{ij}(\mathbf{r})}{\partial\xi_k\partial\xi_l}\int \xi_k\xi_l f_j(\boldsymbol{\xi})d\boldsymbol{\xi} + ... \tag{1.7}$$

Since the swimmer is force free we get that the first monopole term cancels out, making the leading term dipolar. By analysing the multipole expansion it can be shown that the far field flow for a micro-swimmer is given by [30]:

$$u(\mathbf{r}) = \frac{F}{8\pi\mu}\frac{l}{r^2}(3\cos^2\theta - 1)\hat{\mathbf{r}} \tag{1.8}$$

where θ is an angle defined relative swimming direction $\mathbf{p}$ and $\hat{\mathbf{r}}$ is a unit vector in the direction of $\mathbf{r}$. The expression given in Eq 1.8 is called a stresslet, and can be considered as the directional derivative of the stokeslet and is obtained in the limit when two point forces, pointing in the opposite direction approach each other. One can classify the stresslet expression into two cases; a *puller* is a stresslet field where the point-forces point towards each other, a *pusher* is a stresslet where they point away from each other. In Eq 1.4 in terms of the flow field this translates to $F > 0$ and $F < 0$ for pushers respectively pullers.

Pushers will eject fluid along their main swimming axis, and pull in fluid from the sides, whereas pullers do the opposite. The transition from outward to inward flow happens at a fixed angle relative to the swimming direction $\mathbf{p}$ of $\arccos(\frac{1}{\sqrt{3}})$. The type of stresslet that best approximates the flow filed of a certain swimmer is dependent on swimming strategy: *E. coli* bacteria are for instant pushers whereas *C. reinhardtii* algae are pullers [12, 30]. Figure 1.3 and Figure 1.4 shows a typical pusher respectively puller flow field.

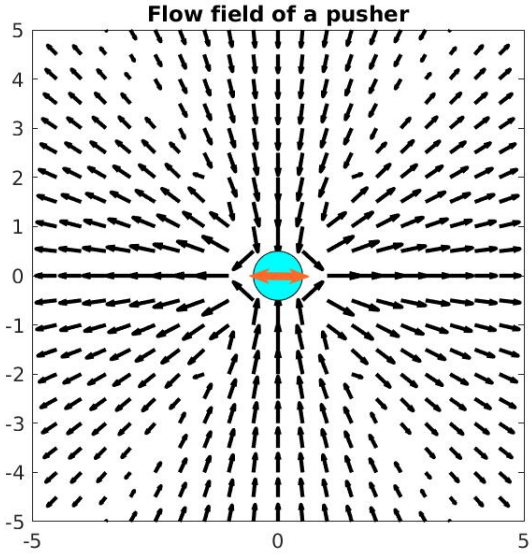

Figure 1.4: A flow field due to a pusher, the length of the vectors have been scaled logarithmically

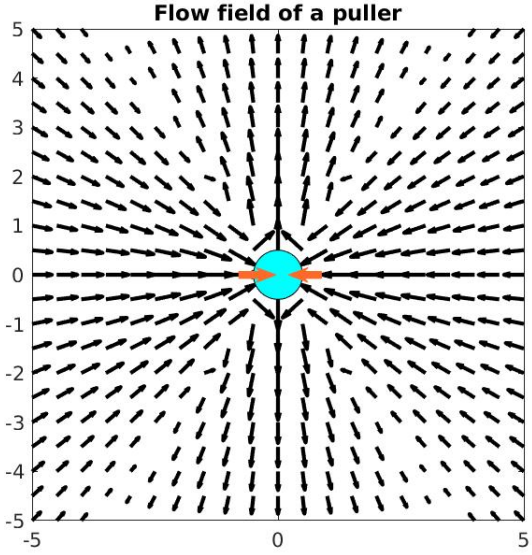

Figure 1.5: A flow field due to a puller, the length of the vectors have been scaled logarithmically

1.3 Active turbulence

In this section we will review some theories and experimental findings that occur in suspension consisting of many microswimmers. Microorganisms exist in every part of the biosphere, from archea in the depths of the oceans or inside our bodies as either harmful or beneficial bacteria. They also play a central role in many biological and ecological processes in nature, such as digestion, reproduction and CO_2 capture and mixing in the oceans [17]. Understanding the motility, dynamics and interactions in collections of swimming microorganisms is therefore crucial in order to accurately model these aforementioned phenomena. Furthermore, the findings made from these studies might also be generalized to artificial microswimmers, that might be used for future technological applications.

As we saw in the previous section, each microswimmer sets up a flow field that decays slowly with the distance from the swimmer. This in turn results in strong particle-particle hydrodynamic interaction which may cause exotic behaviours in suspension of many swimmers. Experimental findings have for instance been made by Goldstein et al [3]. Suspensions of *B. subtilis*, a pusher type swimmer, was analysed with the help of particle-imaging-velocimetry. Though being in the low Reynolds regime, these suspensions show properties that are typical for turbulent flows: jets, eddies and coherent regions that might last for seconds. This turbulent state, which occurs in dense enough suspensions of pusher microswimmers, display a rich variety of properties such as enhanced swimming speed, higher diffusivity of passive tracer particles and emergence of patterns and density fluctuations. Similar studies have also been made for suspension of *E. coli* and for artificial system consisting of microtubules and dynein, all of which exhibit flow fields with pusher symmetry [7, 22].

Figure 1.6: Accumulation of *B. subtilis* cells at the slop of an air/water interface, the bacteria exhibit collective motion. The black speckles are latex particles 2 micrometer in size. Image reproduced from Ref.[3]

Theoretical studies have also been done to account for these findings. One approach is to use kinetic theory [21, 20, 18, 25]. In this type of model, one defines a probability distribution function for the N-body system
$\Psi(\mathbf{r}_1, ..., \mathbf{r}_N, \mathbf{p}_1, ..., \mathbf{p}_N, t)$ describing the probability during time t to find the center of mass $\mathbf{r_i}$ and swimming direction $\mathbf{p}_i$ of the i:th swimmer. It is normalised according to :

$$\frac{1}{V}\int_V \int_\Omega \Psi(\mathbf{r}_1, .., \mathbf{r}_N, \mathbf{p}_1, .., \mathbf{p}_N, t) d\mathbf{r}_1 .. d\mathbf{r}_N d\mathbf{p}_1 ... d\mathbf{p}_N = \rho, \tag{1.9}$$

where V is a volume, Ω is the unit sphere and ρ is the number density. Since the number of swimmers are conserved, it can be shown that Ψ should obey a Smoluchowski equation:

$$\frac{\partial \Psi}{\partial t} + \nabla_x \cdot (\dot{\mathbf{x}}\Psi) + \nabla_p \cdot (\dot{\mathbf{p}}\Psi) = 0 \tag{1.10}$$

where ∇_p is the gradient on the unit sphere. Here $\dot{\mathbf{x}}$ and $\dot{\mathbf{p}}$ represents the center-of-mass velocity and the rotational flux velocity respectively. In order to close the Smoluchowski equation one proceeds by defining an equation of motion for the swimmers and one equation for the fluid-dynamics. From these models it can be shown that densities exceeding the critical density $\rho_c \equiv 5\lambda/\kappa$, where λ is the tumbling frequency and κ is the dipole strength of the stresslet field, give rise to hydrodynamic instabilities for pushers, whereas pullers are stable.

Another class of models, that starts from the equations describing liquid crystals, modified by including an active stress that is due to the microswimmers, results in so-called active nematics [5, 16, 27]. The nematic order and its magnitude and orientation are described with a second rank traceless tensor Q_{ij}, from which one can define an equation that describes how Q_{ij} interacts with the fluid, and how it relaxes to a free energy minimum. The model is finally obtained by coupling the evolution of Q_{ij} to a modified NSE that includes a term containing the active stress. Under certain condition these models also display hydrodynamic instabilities. The generation and destruction of topological defects have been observed in this systems.

A few particle-based studies of active turbulence have also been performed [29, 19, 11]. Simulations provide a way to test the aforementioned continuum theories under conditions that cannot be achieved in experiments. Compared to the continuum models described above, these simulations also reveals fluctuations that result from the discrete nature of the swimmers and furthermore enables the exploration of interactions between different type of swimmers, tracer particles and boundries that have not yet been incorporated in continuum theories [11].

1.4 Questions and aims

Most of the previous mentioned studies only consider one type of microswimmer, while the collective behaviour of binary mixtures between pushers and pullers is still a relatively uncharted territory. In this thesis we will investigate the collective behaviour of binary pusher and puller mixtures by means of particle-based simulations. Questions that we wish to address in this thesis are :

- What characteristics will the two body interaction give rise to in swimmer pairs? Is it repelling, aligning or attractive?
- How does the fraction of different swimmer types affect the transition to collective dynamics?
- How does doping with a small amount of pullers effect the turbulent state in a pusher suspension?
- To what extent is self-propulsion relevant for the observed collective behaviours? How do non-swimming particles behave?

The only previous study of pusher-puller mixtures considers a 2-dimensional system of microswimmers with hydrodynamic interactions and steric repulsion [14]. This thesis will instead focus on 3 dimensional systems and only consider hydrodynamic interactions. With our model we are able to simulate up to $\sim 10^6$ particles, which lies in the region of biologically relevant numbers.

Chapter 2

Model and Methods

This chapter will introduce the necessary theory and concept needed to understand the tools used for this thesis. In the first section we will discuss the equation of motion for the swimmers and how they interact with the fluid and each other. The hydrodynamic of the system is governed by the NSE. In the second section of this chapter we will provide a brief account on how the Lattice Boltzmann Method (LBM) can be used to solve it. The third section will discuss the details of our simulations.

2.1 Model

Our model considers a 3-dimensional suspension of N swimmers immersed in fluid inside a box with periodic boundaries with volume $V = L^3$ and a number density of $\rho = N/V$. Each particle is modelled as an extended force dipole (also known as extended stresslet), the body and flagella exert two equal but opposite forces $\pm F\mathbf{p}$ where F is the magnitude of force, and $\mathbf{p}$ is the swimming orientation. The forces are separated by a length l. The swimmers are characterized by a dipole strength $\kappa \equiv \pm Fl/\mu$ where μ is the fluid viscosity, with $\kappa < 0$ representing pullers and $\kappa > 0$ pushers. The position $\mathbf{r}$ and orientation $\mathbf{p}$ evolve according to the following equations of motion :

$$\dot{\mathbf{r}} = v_s\mathbf{p} + \mathbf{U}(\mathbf{r}), \tag{2.1}$$

$$\dot{\mathbf{p}} = (\mathbb{I} - \mathbf{pp}) \cdot (\nabla\mathbf{U}) \cdot \mathbf{p} \approx (\mathbb{I} - \mathbf{pp}) \cdot \frac{\mathbf{U}(\mathbf{r}) - \mathbf{U}(\mathbf{r} - \mathbf{p}l)}{l}, \tag{2.2}$$

here, v_s is the constant swimming velocity that the swimmer propels itself with, and $\mathbf{U}(\mathbf{r})$ is the fluid velocity evaluated at the swimmer position. Eq. 2.2 is Jeffery's equation for infinite aspect ratio ($\beta = 1$). It is widely used in the theory of suspensions and describes the motion of a ridgid ellipsoidal body immersed in a linear flow [10]. It has been shown that finite aspect ratios ($\beta < 1$) give only

small changes [2]. Apart from being rotated by the fluid in accordance with Eq 2.2, our particles also perform random reorientations according to a run-and-tumble walk. This is done in the form of a Poisson process, with the frequency λ, giving the swimmers a persistence length of v_s/λ. In order to treat the fluid flow $\mathbf{U}(\mathbf{r})$, created by the collection of swimmers we need to solve the Navier-Stokes equation. An implementation of the Lattice Boltzmann method is used for that purpose, and is the topic of the next section.

2.2 The Lattice Boltzmann method

We will in this section give an introduction to the LBM, the derivation is mostly based on the book written by Krüger et al [28].

2.2.1 Boltzmann Equation

The LBM builds on the ideas of kinetic theory and is a mesoscopic method, i.e it tracks the evolution of fictive particles using distributions. In the kinetic theory of monoatomic gases one models gases by a distribution function $f(\mathbf{x}, \xi, t)$ were $\mathbf{x}$ is position, ξ is velocity and t is time. The moments of f in velocity space corresponds to useful macroscopic quantities, for instance we have that

Density ρ:

$$\rho = \int f(\mathbf{x}, \boldsymbol{\xi}, t) d\boldsymbol{\xi}, \tag{2.3}$$

Momentum density $\rho\mathbf{u}$:

$$\rho\mathbf{u} = \int \boldsymbol{\xi} f(\mathbf{x}, \boldsymbol{\xi}, t) d\boldsymbol{\xi}, \tag{2.4}$$

Total energy density $E\mathbf{u}$:

$$E\mathbf{u} = \frac{1}{2} \int |\boldsymbol{\xi}|^2 f(\mathbf{x}, \boldsymbol{\xi}, t) d\boldsymbol{\xi}, \tag{2.5}$$

The equation governing the evolution of the distribution function f is the Boltzmann Equation (BE), which takes the following form :

$$\frac{\partial f}{\partial t} + \xi_\beta \frac{\partial f}{\partial x_\beta} + \frac{F_\beta}{\rho} \frac{\partial f}{\partial \xi_\beta} = \Omega(f), \tag{2.6}$$

The first two terms in the equation accounts for the advection that the distribution functions experiences due to the velocity of its particles. The third term accounts for forces F_β effecting the velocities. The right hand side corresponds to a collision operator $\Omega(f)$, it accounts for local redistribution due to collisions.

There are many different collision operators, all good for different applications, however in the context of Lattice-Boltzmann simulations one usually adopts the Bhatnagar-Gross-Krook (BGK) operator:

$$\Omega_i(f_i) = \frac{f_i(\mathbf{x},t) - f_i^{eq}(\mathbf{x},t)}{\tau}, \tag{2.7}$$

Where f_i and f_i^{eq} are the discrete distribution function and the discrete equilibrium distribution function respectively. The index i symbolises that we only are considering particles with a specific velocity $\mathbf{c}_i$. τ is a relaxation time. It can be shown that the equilibrium distribution function obeys a Maxwell-Boltzmann distribution law :

$$f^{eq} = \rho \left(\frac{1}{2\pi RT} \right)^{3/2} e^{|\mathbf{v}|^2/2RT}, \tag{2.8}$$

where R is the gas constant, and v is the particle velocity.

The main idea behind the LBM is that the BE and NSE are different description of the same underlying physical phenomenon. This can be shown by performing a perturbation expansion, a so called Chapman-Enskog analysis. This is however beyond the scope of the text. A thorough derivation relating the BE to the NSE is given in [28, 26]. In the proceeding we will derive the discretized version of the BE, the so called Lattice Boltzmann equation, and give an account of how it is used in computer simulations.

2.2.2 The Lattice Boltzmann Equation

To solve the BE numerically, we need to discretize Eq 2.6. The discretization step is a rather cumbersome and a thorough walk through is beyond the scope of this thesis, but we wish to lay out a brief guideline for how one might do this. The procedrure involves one discretization in velocity space and one discretization in space and time. Henceforth we assume that Eq. 2.6 is force free, that we have a BKG collision operator and that the fluid is isothermal.

The velocity space discretization builds on Hermite polynomial (HP) expansion of the distribution function. Since the HP:s span a Hilbert space, given a sufficiently well behaved function one might write f as an infinite linear combination of HP [23], we have that :

$$f(\mathbf{x},\boldsymbol{\xi},t) = \omega(\boldsymbol{\xi}) \sum_{n=0}^{\infty} \frac{1}{n!} \mathbf{a}^{(n)}(\mathbf{x},t) \cdot \mathbf{H}^{(n)}(\boldsymbol{\xi}), \tag{2.9}$$

were $\omega(\boldsymbol{\xi}) = \frac{1}{\sqrt{2}} e^{-|\boldsymbol{\xi}|^2/2}$ is the generating function of the HP:s, $\mathbf{H}^{(n)}$ is the n:th HP and $\mathbf{a}^{(n)}$ is the expansion coefficient of the n:th term given by:

$$\mathbf{a}^{(n)}(\mathbf{x},t) = \int f(\mathbf{x},\boldsymbol{\xi},t)\cdot\mathbf{H}^{(n)}(\boldsymbol{\xi})d\boldsymbol{\xi}, \tag{2.10}$$

Both $\mathbf{H}^{(n)}$ and $\mathbf{a}^{(\mathbf{n})}$ are tensors of rank n.

By expanding the equilibrium distribution function given in Eq 2.8 in this basis one finds that the first three terms respect the conservation of mass, momentum and energy. This justifies truncation of f^{eq} to only three terms and we can thus approximate f^{eq} to:

$$f^{eq} \approx \omega(\xi)\rho Q(\boldsymbol{\xi}), \tag{2.11}$$

where $Q(\boldsymbol{\xi})$ is a multi-dimensional polynomial. One useful property of the HP:s for numerical integration is the Gauss-Hermite Quadrature rule: given an 1-dimensional polynomial of order n, $P^n(x)$, one can calculate the integral $\int \omega(x)P^n(x)dx$ by considering the values of the integrand in some discrete points x_i corresponding to the zeros of the HP:s :

$$\int_{-\infty}^{\infty}\omega(x)f(x) = \sum_{i=1}^{n} w_i f(x_i) \tag{2.12}$$

where w_i are weighting coefficients. This can easily be extended to several dimension.The expansion coefficients of the equilibrium distribution function $\mathbf{a}^{(n),eq}$ are thus:

$$\mathbf{a}^{(n),eq} = \int \omega(\boldsymbol{\xi})\rho Q(\boldsymbol{\xi})\cdot\mathbf{H}^{(n)}(\boldsymbol{\xi})d\boldsymbol{\xi} = \sum_{i=1}^{n} w_i Q(\xi_i)\mathbf{H}^{(n)}(\xi_i) \tag{2.13}$$

An implication of the last equality is that we only need a finite set of velocities to calculate the integral. By choosing the velocities according to the Gauss-Hermitte Quadrature rule one can construct a velocity set $(\mathbf{c}_i, w_i)$. By doing this we have discretized velocity space while still respecting the laws of conservation. Before we proceed with the space and time discretization a word on velocity sets is needed. A velocity set is not unique and several sets can be constructed. A common notation used for referring to velocity sets is the DdQq system, were d is the dimensionality and q is the number of velocities.

A higher resolution is obtained with more velocity components, making it possible to consistently solve the NSE. However there is a trade-off; the computational cost grows with the number of velocity components. It is therefore important that one finds a set with a minimum number of velocities, yet with the ability to capture the desired physics. Figure 2.1 shows an illustration of a few velocity sets.

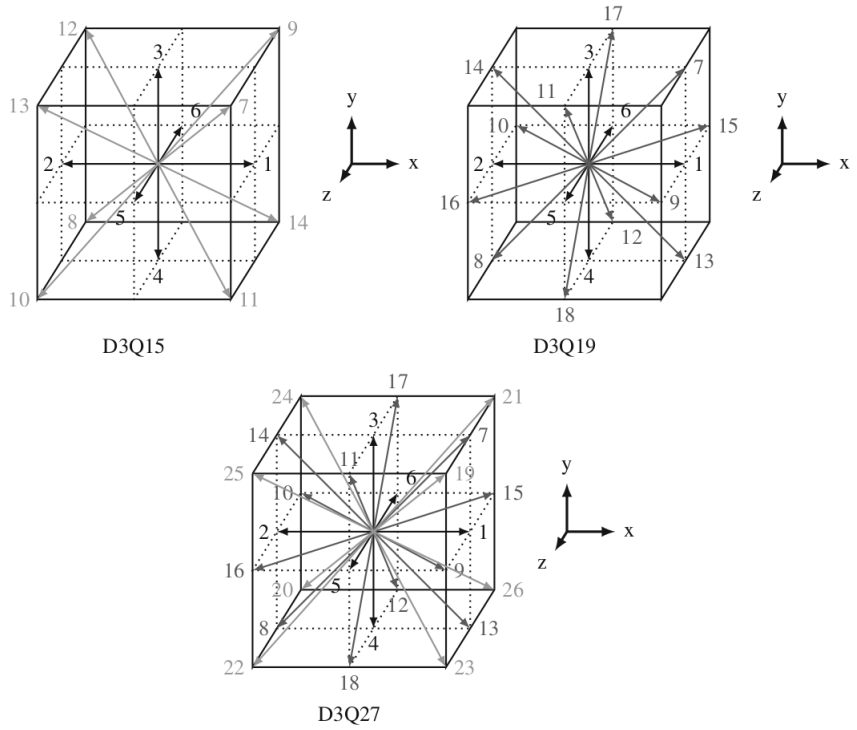

Figure 2.1: An illustration of a number of velocity sets in 3 dimensions. Having more velocity components can increase accuracy of the simulation however this comes at the price of numerical costs. Image reproduced from Ref. [28].

After discretizing in velocity space we obtain the discrete-velocity Boltzmann equation :

$$\frac{\partial f_i}{\partial t} - c_{i\alpha}\frac{\partial f_i}{\partial x_\alpha} = \Omega_i(f_i) \tag{2.14}$$

Where $f_i = f(\mathbf{x}, \mathbf{c}_i, t)$ is the discretized distribution function and $\Omega_i(f_i)$ is the corresponding BGK collision operator. The reader familiar with partial differential equation might have noticed that Eq. 2.14 is a first-order hyperbolic partial differential equation. The method of characteristics might be used to solve these. This allows us to parametrize the independent variables in such away that the PDE can be cast into a ordinary differential equation. A solution to 2.14 can be written in the form $f_i = f_i(\mathbf{x}(\eta), t(\eta))$ were η traces out an trajectory in space and time. Inserting this into Eq. 2.14 we get:

$$\frac{\partial f_i}{\partial \eta} = \frac{\partial f_i}{\partial t}\frac{\partial t}{\partial \eta} - \frac{\partial f_i}{x_\alpha}\frac{\partial x_a}{\partial \eta} = \Omega_i(\mathbf{x}(\eta), t(\eta)) \tag{2.15}$$

Eq. 2.14 requires that we chose a trajectory fulfilling $\frac{\partial t}{\partial \eta} = 1$ and $\frac{\partial x_\alpha}{\partial \eta} = c_{i\alpha}$. We have now obtained an ordinary partial differential equation. To proceed we need to integrate along the trajectory, resulting in:

$$f_i(\mathbf{x} + \mathbf{c}_i\Delta t, t + \Delta t) = \int_0^{\Delta t} \Omega_i(\mathbf{x} + \mathbf{c}_i\eta, t + \eta)d\eta \tag{2.16}$$

The left hand side is easy to calculate, it follows from the fundamental theorem of calculus. The right hand-side is a bit harder to determine. By using approximation schemes, that are beyond the scope of this text, one might approximate the integral. The final expression for the fully discretized BE is :

$$f_i(\mathbf{x} + \mathbf{c}_i\Delta t, t + \Delta t) = f_i(\mathbf{x}, t) - \frac{\Delta t}{\tau}(f_i(\mathbf{x}, t) - f_i^{eq}(\mathbf{x}, t)) \tag{2.17}$$

One can break down the equation in to two distinct parts. On the right hand side we have the collision step :

$$f_i^* = f_i(\mathbf{x}, t) - \frac{\Delta t}{\tau}(f_i(\mathbf{x}, t) - f_i^{eq}(\mathbf{x}, t)) \tag{2.18}$$

where f_i^* is f after collision. This accounts for changes in position and velocity due to particles colliding on the lattice. The left hand side describes the propagation step and shows how f_i^* should be redistributed:

$$f_i(\mathbf{x} + \mathbf{c}_i\Delta t, t + \Delta t) = f_i^* \tag{2.19}$$

By iteratively going thorough equation Eq. 2.18 and Eq. 2.19 one can generate different values of f_i. Since mass and momentum still is conserved, one might calculate values of ρ and $\mathbf{u}$ from the moments of f_i

$$\rho = \sum_i f_i \tag{2.20}$$

$$\rho\mathbf{u} = \sum_i \mathbf{c}_i f_i \tag{2.21}$$

The steps layed out so far do not consider any force terms. In the derivation given above, we assumed that Eq. 2.6 was force free. One can derive a similar numerical scheme for the forced case, see for instanace [28, 13]. Given that we can account for forces, we still need to incorporate them into the simulation somehow, something that we will discuss next.

2.2.3 Interpolation of forces

The swimmers used in our simulation, as mentioned earlier, are modelled as extended force-dipoles, i.e. as point forces separated by a distance l. We assume that the swimmers are moving off lattice, which enables us to simulate far higher amount of swimmers. In order to do this we need a way to interpolate the forces from the swimmers on to the lattice. Following Nash et al [13] one can use a regularized Dirac δ function, a so called Peskin Delta function δ^p. It is given by:

$$\delta^p(\mathbf{r}) = \frac{1}{h^3} f(\frac{x}{h}) f(\frac{y}{h}) f(\frac{z}{h}) \tag{2.22}$$

Where $h = \Delta x = \Delta y = \Delta z$ is the lattice spacing and $f(r)$ is given by:

$$f(r) = \begin{cases} \frac{3-2|r|+\sqrt{1+4|r|-4r^2}}{8} & \text{if } \mid r \mid \leq 1 \\ \frac{5-2|r|+\sqrt{-7+12|r|-4r^2}}{8} & \text{if } 1 \geq \mid r \mid \leq 2 \\ 0 & \text{if } \mid r \mid \geq 2 \end{cases} \tag{2.23}$$

Using δ^p one can include forces onto the lattice and then solve the forced LBE. Doing this we are able to account for the dipole field that the swimmers exert on the fluid. In a similar manner we can interpolate velocities from the lattice to the swimmers.

2.3 Simulations and units

An in house developed software called LBSWIM was used to simulate the swimmer suspensions. LBSWIM is written in FORTRAN and implements a D3Q15 BGK LBM with point forces implemented according to Nash et al [13]. The swimmers were modelled as extended force dipoles. These forces give rise to flow fields by which the swimmers rotate and advecte each other according to the equations of motions Eq. 3.1 and Eq. 3.2. It is important to notice that *no* excluded volume interaction or near filed hydrodynamics is taken in to account in our simulations. All simulations were performed in a periodic box, with the length $L = 100$. The number of swimmers N were varied between the simulations, which also changed the number density, defined as $\rho \equiv \frac{N}{L^3} = \frac{N}{V}$ with V being the volume of the box. The number of pusher respective pullers were also varied between simulations, the fraction of pullers denoted X was used to characterize the ratio between the different swimmers in each simulations. Unless mentioned otherwise, the swimmers started with random values of $\mathbf{p}$ and $\mathbf{r}$.

In a Lattice Boltzmann simulation, the properties of the lattice are used to create a specific set of units, where the lattice spacing and the time step are used as the basic units of length and time, respectively. In terms of these units we have the following values on our parameters: $v_s = 10^{-3}$, $F = 1.57 \cdot 10^{-3}$, $l = 1$, $\lambda = 2 \cdot 10^{-4}$ and $\mu = 1/6$, with the latter value corresponding to the fluid relaxing to local equilibrium on each timestep. As mentioned earlier, we also have the dipole strength as $\kappa = Fl/\mu$. The value of the aforementioned parameters were made so that they would resemble *E. coli*. To simplify things we define the non-dimensionalized dipole strenght as $\kappa_n = \kappa/(l^2 v_s)$. Except from a few cases, all swimmers had $\kappa_n \approx 9.4$., this is comparable to *E. coli*, were we have $\kappa_n \approx 11$ [2].

To make the presentation of our results more intuitive we defined new units for time and length. The unit of time was defined with respect to the swimming velocity v_s. One time unit corresponds to the time it takes for a swimmer to move one lattice spacing with velocity v_s. The unit of length was defined according to the stresslet separation length l which was chosen to be 1 lattice separation.

Chapter 3

Results and Discussion

The aim of this chapter is to present the results of our simulations. These were performed for different values of density ρ and swimmer fractions X. Results regarding two body interaction, fluid statistics and swimmer statistics will be discussed for mixtures of pushers and pullers. Similar studies were also performed for binary pusher and puller suspensions consisting of shakers. The aim is to study the onset to collective motion and its dependence on the composition of the suspension and the similarities and differences between swimmers and shakers.

3.1 Two-particle collisions

The chaotic flows encountered during active turbulence display length and timescales much larger than the individual microswimmer. This phenomenon has been attributed to the hydrodynamic interactions between the swimmers, through which swimmers reorient each other [24]. The simplest type of interaction that one might study is the interaction between an isolated pair of microswimmers. Within this section we wish to highlight the dynamics of two-body interaction of pushers and pullers.

Each swimmer is described by its position $\mathbf{r}$ and swimming direction $\mathbf{p}$, chosen in a way such that they will collide in the center of the box. The initial angle between the swimming directions was set to be 45°. These simulations where performed for three type of pair interactions; pusher-pusher, puller-puller, and pusher-puller.

To make the swimming trajectories deterministic the random reorientations of the swimmers were omitted. To further enhance the interaction we increased the non-dimensionalised stresslet strenght to $\kappa_n = 36$, which is about four times bigger than the corresponding non-dimensionalised stresslet strenght of *E. coli*. The resulting time dependent distance between the swimmers and their angle between the swimming directions as a function of time are presented in Figure 3.1.

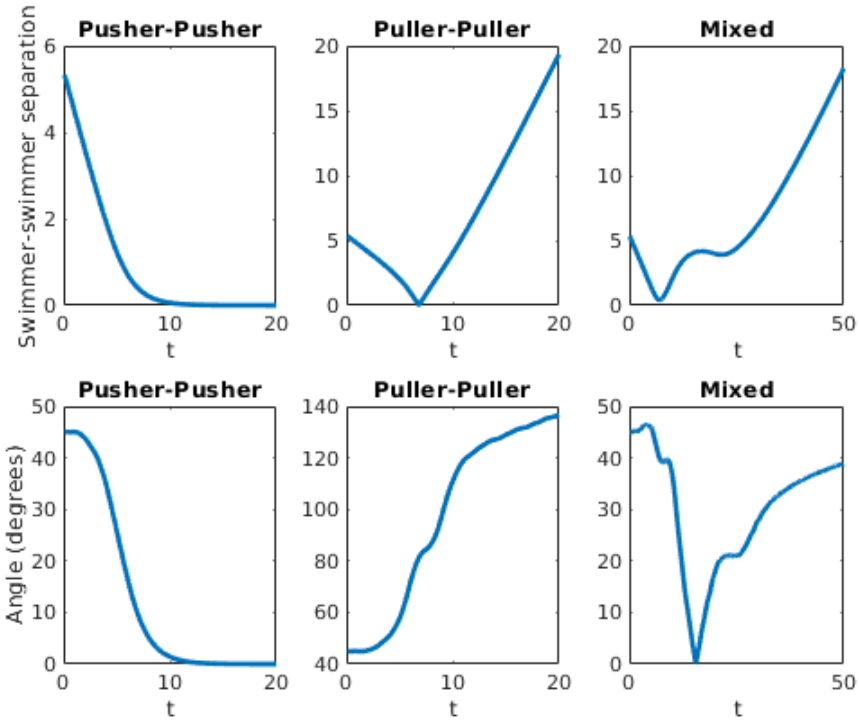

Figure 3.1: Swimmer-swimmer distance (first row) and the angle between the swimmer direction (second row) as a function of time, respectively. Notice the difference to scale

From simulations one can see that pushers align with each other; as shown in Figure 3.1 both the angle and the distance approaches zero after the collision. The opposite trend holds for pullers, the interaction reorients the swimmers to an anti-parallel configuration, making them swim away from each other with an increased speed after the collision. The tendency for alignment and anti-alignment might explain why active turbulence only occur for pushers and is absent in puller suspensions.

Further insights might be obtained from studying the flow-field from a single point stresslet. The fluid flow induced at a point $\mathbf{r}$ with respect to the swimmer positioned at the origin, with an angle θ relative to the stresslet orientation is given by

$$u(\mathbf{r}) = \frac{F}{8\pi\mu}\frac{l}{r^2}(3\cos^2\theta - 1)\hat{\mathbf{r}} \tag{3.1}$$

Where $r = |\mathbf{r}|$ and $\hat{r} = \mathbf{r}/r$ and F is the magnitude of the force, with $F > 0$ for pushers and $F < 0$ for pullers . For side-by-side swimming ($\theta = 90$ °), a relative velocity scaling of $\sim -F/(\mu r^2)$ occurs. Two pushers will therefore induce a drag on each other which attracts them laterally, whereas two puller induce a laterally repelling drag. For a head to tail alignment of swimmers ($\theta = 0°$) the velocity is depends as $\sim F/(\mu r^2)$, giving the opposite attraction and repulsion [12].

For the mixed pusher-puller interaction we no longer have action-reaction symme-

try; the two swimmers will exert flow fields that differ from each other by a change in sign (assuming they have the same magnitude of F). From Figure 3.1 we can see that the mixed interaction initially leads to a decrease in the angle between the swimming directions, but as time progresses the alignment breaks and the swimmers drift away. The highly non-monotonic behaviour of the angel between the swimming direction seem to indicate that neither alignment or anti-alignment will occur. This in turn means that active turbulence might be present to some extent. Due to the different nature of the two-body interactions it seems likely that the ratio of pushers and pullers will play a role in mixed suspensions of both pushers and pullers.

3.2 Microswimmers: Fluid statistics

In order to investigate the consequences of the two-body interactions from the previous section we will now consider a 3-dimensional suspension.

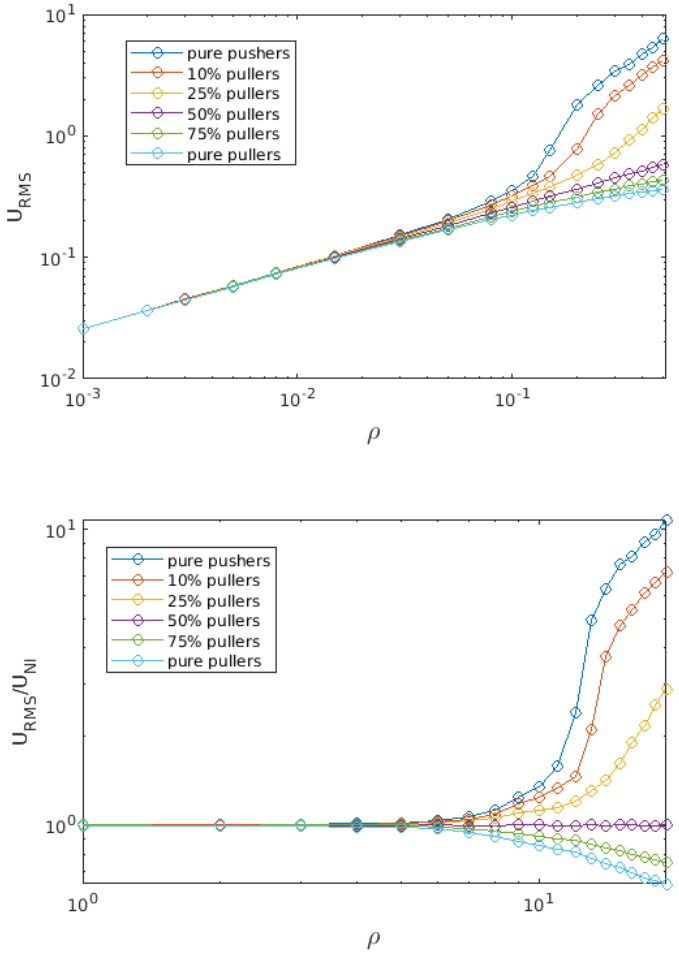

Figure 3.2: Top: U_{RMS} as a function of density in mixtures between pusher and puller swimmers. Bottom: The U_{RMS} value rescaled by the corresponding value in the non interacting system U_{NI}

The onset to collective behaviour can be observed through the root mean square (RMS) fluid velocity $U_{RMS} \equiv \langle U^2 \rangle^{1/2}$ as a function of ρ [24]. Figure 3.2 shows U_{RMS} vs ρ for different values of X. In the dilute region, interactions between swimmers are negligible, corresponding to an effective dynamics where the terms containing $\mathbf{U}$ in Eq. 3.1 and Eq. 3.2 are set to zero. In this limit the swimmers

become statistically independent which makes the task of deriving analytical results much simpler. From theoretical studies it is known that $U_{NI} \propto \rho^{1/2}$ which is in accordance with the low-density scaling observed in Figure 3.2 [2]. As the suspension gets denser the hydrodynamic interactions become more relevant and we observe the onset to collective motion in the pure pusher suspension. It is clear that the pullers have a disrupting effect on the collective dynamics, and that it is non-additive in its effect on U_{RMS}. The transition to collective motion only occurs for suspensions were pushers outnumber pullers, our data shows that $X = 0.75$ is the minimum fraction where we observe no transition to collective motion. However, from its linear shape, it also seems as if $X = 0.5$ might be a strict limit for the emergence of turbulence, meaning that all values $X > 0.5$ will not give rise to turbulence. From the looks of it it also seems as if the $X = 0.5$ overlaps quite well with the low density behaviour.In order to further quantify this observation, we plot the *normalized* RMS fluid velocity, obtained by dividing U_{RMS} value with the corresponding value for non-interacting swimmers. The result is reported in Figure 3.2. In spite of the presence of interactions, the $X_p = 0.5$ data *perfectly* reproduces the same RMS fluid velocity for non-interacting swimmers at the same density.

The chaotic flows displayed during active turbulence can be further characterized by their length- and timescales. In order to proceed, we define the spatial correlation function $c(r)$ and the auto correlation function $c(t)$ of the fluid velocity $\mathbf{U}(\mathbf{r}, t)$:

$$c(r) \equiv \frac{\langle \mathbf{U}(\mathbf{0}) \cdot \mathbf{U}(\mathbf{r}))\rangle}{\langle \mathbf{U}^2 \rangle} \tag{3.2}$$

$$c(t) \equiv \frac{\langle \mathbf{U}(0) \cdot \mathbf{U}(t)\rangle}{\langle \mathbf{U}^2 \rangle} \tag{3.3}$$

In Figure 3.3 we show $c(r)$ and $c(t)$ for different values of X. The spatial correlation function and auto correlation behave differently. However, a common trend is that pusher dominated suspensions show slower overall decay compared to its puller dominated counterparts. It is not yet obvious if these functions obey an analytical expression. In order to quantitatively measure the length-and timescales of the fluid flow we thus define the characteristic lengthscale ξ as the distance were $c(r)$ has decayed to 0.2, whereas the timescale τ is defined as the time were $c(t)$ has decayed to 0.4. The timescale has a higher threshold value due to the slow dynamics around the transition density; it decays to 0.2 far too slowly, making the statistics poor.

The lengthscale ξ and timescale τ reported as a function of density are presented in Figure 3.4. In the case of the pure pusher suspension we can see an increase around the transition to turbulence $\rho = 0.15 - 0.2$. In the case for U_{RMS} we see a transition to active turbulence for suspensions with more than 50% pushers. The $X = 0.1$ suspension deviates from the pure pusher suspension in the dilute region, however in the dense region there seems to be no significant change. However it seems as if small amount of doping shifts the transition value density, in accordance with the results presented above. The $X = 0.25$ suspensions exhibits a rather different behaviour compared to the other pusher dominated suspensions, in that it increases monotonically whereas the former have a non-monotonic behaviour with a rather diffuse maximum. For the puller dominated suspensions we have no active turbulence and it seems as if there is a slight decrease in ξ with ρ.

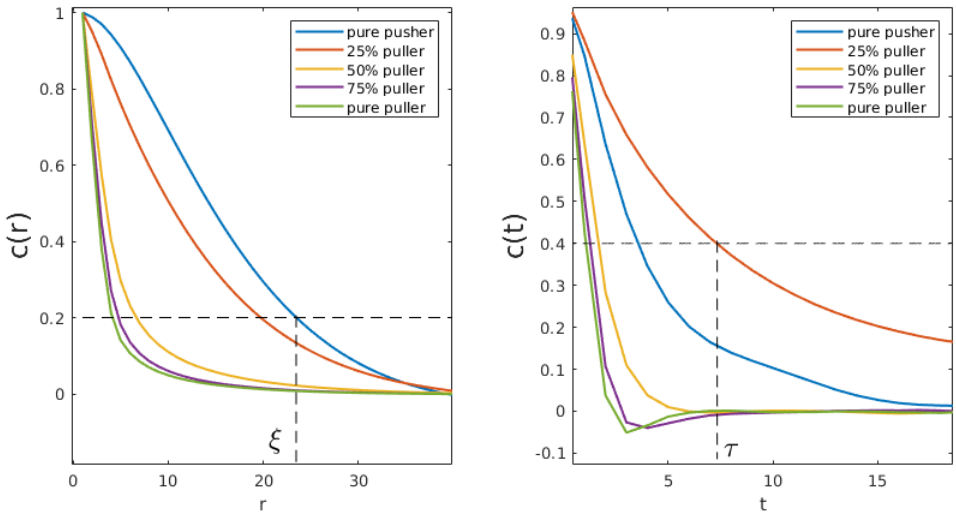

Figure 3.3: Left: The spatial velocity function $c(r)$ for different values of X,the dashed line demonstrates the definition of ξ. Right: The auto correlation function $c(t)$ for different values of X, the dashed line demonstrates the definition of τ. $\rho = 0.5$ for all correlation functions

Regarding τ, a distinct maximum can be seen for the pusher dominated suspensions. Doping with pullers speeds up the dynamics and it also shifts the maximum corresponding to the transition horizontally. In the case of the pure pusher suspension ($\rho = 0.15$) and $X = 0.10$ ($\rho = 0.25$) the shift in maximum corresponds to $\sim 70\%$, suggesting that the presence of pullers have a strong and nonlinear disrupting effect on the collective motion.

ξ shows no variation with density for $X = 0.50$, again highlighting the equal part suspensions properties with the non-interacting case.

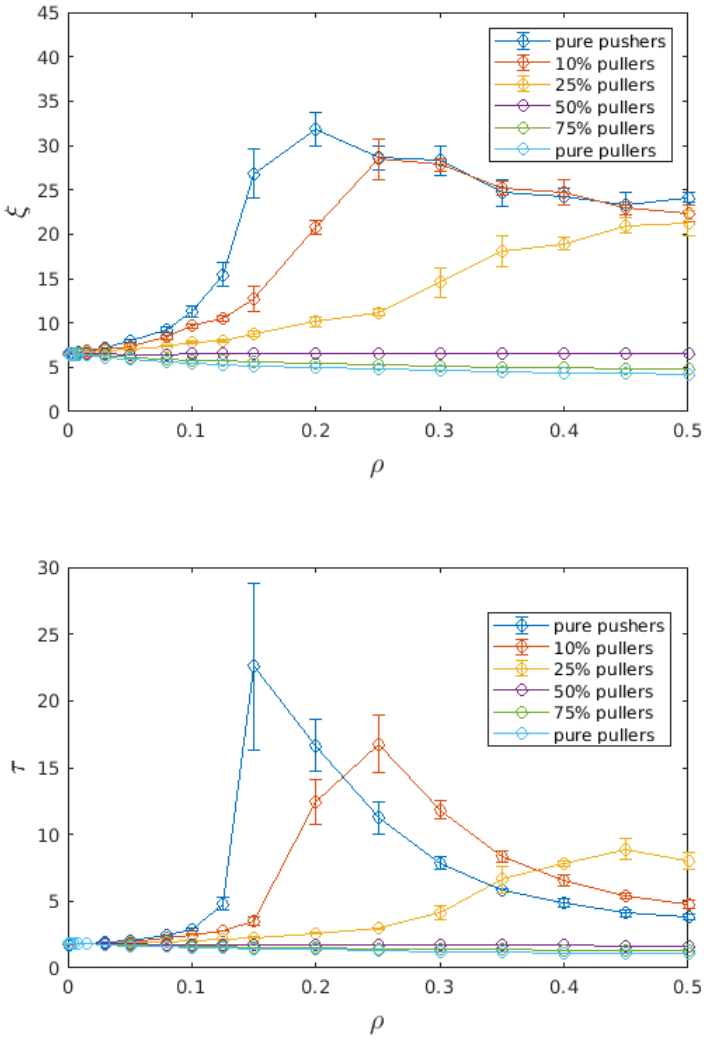

Figure 3.4: The lengthscale ξ (top) and the timescale as τ (bottom) a function of ρ for different values of X.Error-bars were obtained $X < 0.5$ by subaveraging over 4 intervals.

3.3 Microswimmers: Swimmer statistics

In section 4.1 we studied the effect of hydrodynamic pair interactions. We saw that pushers aligned themselves with each other, whereas pullers did the opposite. Microswimmer suspensions consist of many swimmers and the slow decay of the dipole field makes the hydrodynamic interaction long ranged, leading to a complex many body behaviour. In order to generalize the notion of alignment we introduce the local polar order parameter $P(r)$, and the local nematic order parameter $S(r)$:

$$P(r) \equiv \langle P_l(\cos(\theta)\rangle_{|\mathbf{r}_i - \mathbf{r}_j|=r} = \langle \cos(\theta)\rangle_r \tag{3.4}$$

$$S(r) \equiv \langle P_2(\cos(\theta)\rangle_{|\mathbf{r}_i - \mathbf{r}_j|=r} = \left\langle \frac{3\cos^2(\theta) - 1}{2} \right\rangle_r \tag{3.5}$$

Were θ is the angle between the swimming directions of swimmer i and j, positioned at $\mathbf{r_i}$ and $\mathbf{r_j}$. Both order parameters were considered for pusher-pusher, puller-puller and pusher-puller pairs.

The local order parameters are presented in Figure 3.5. The first column in Figure 3.5 shows the results for the pusher-pusher interaction. Local ordering is present for all swimmers fractions. It is however obvious that the introduction of pullers serves to reduce the ordering among the pushers. This effect seems to be more noticeable for the local nematic order parameter. The nematic order parameter also has a longer range compared to the polar order parameter. It is worth pointing out that the stresslet flow field of our swimmers are invariant under a 180°rotation, while the presence of swimming introduces a polar symmetry into the system.

The local order parameter for pullers display a different behaviour. From Figure 3.5 it is evident that (pure)pullers show negative local alignment. This negative alignment has a rather short extent, around 2-3 length units. One possibility for the short range of the anti-alignment is that swimmers who orient each other in to an anti-aligning configuration will repel each other, thus making the interaction short ranged. For suspension with $X < 0.5$ we can see a tendency for local positive alignment a few length units away from the origin. In the case of the $X = 0.1$ we can see a dramatic alignment in the nematic order parameter. An explanation for this is that pushers induce alignment amongst pullers.

The order parameters for the mixed case supports that notion. Both order parameters are positive, and show some similarity with the order parameters for the pusher-pusher case. While the introduction of pullers breaks the alignment between pushers, it seems as if pushers induces nematic order between pullers. For a non-interacting system the order parameters should all be zero. In all order parameters depicted above the $X = 0.5$ suspension shows a small but clear deviation from zero at small swimmer-swimmer separations. This raises the question of what type of configurations the $X = 0.5$ systems takes, and why it produces the same U_{RMS} values as the non-interacting system. One could imagine that on average since there are equal amounts of pushers and pullers, all effects that would lead to alignment and active turbulence from pushers, is countered by the presence of the puller fields. Since no alignment occurs but the particles still set up dipole fields, we effectively get a non-interacting system.

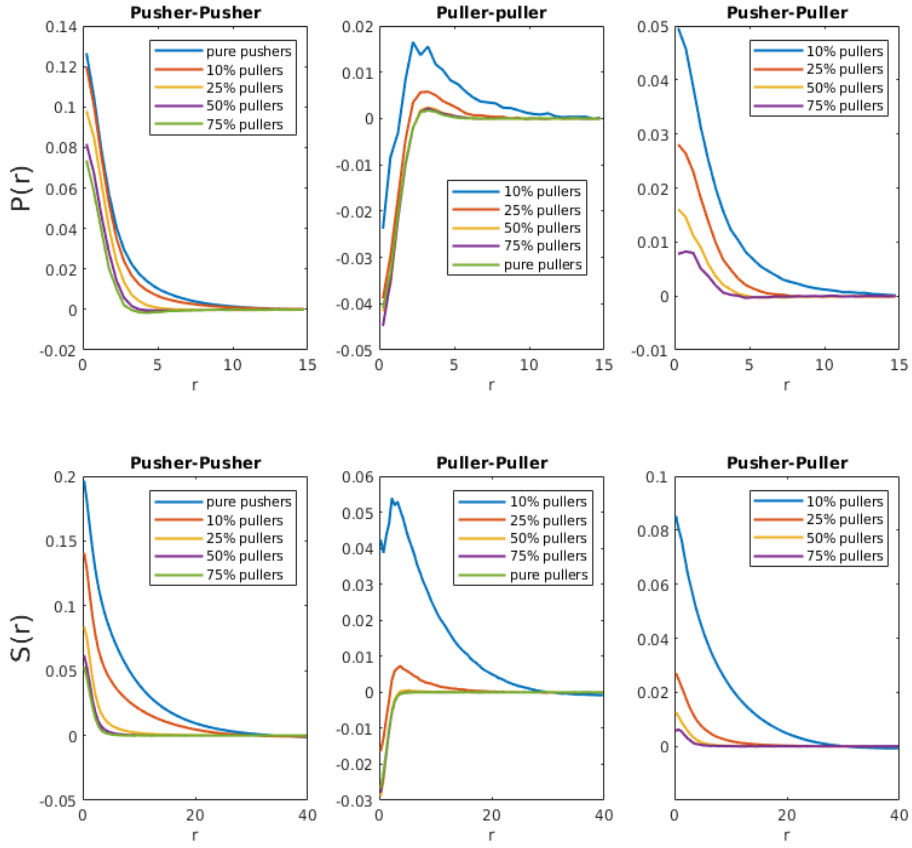

Figure 3.5: The local polar order parameter (top row) and the local nematic order paramter(bottom row) for different interactions.

3.4 Shakers

Shakers are similar to microswimmers in that sense that they *exert* a dipole field on the surrounding fluid. The fluid in turn also rotates and advectes the shakers. The difference is that shakers *do* not swim, i.e. they do not propel themselves along the swimming direction **p**. An implementation of a shaker could for instance be two spheres, attached to each other through a rod, exerting equal but opposite forces. As a model for biological microswimmers this might seem like a severe simplification; locomotion is a fundamental ability of microorganisms. However it opens up the possibility for more in depth theoretical analysis while still exhibiting many of the fascinating collective behaviours observed in microswimmer suspensions.

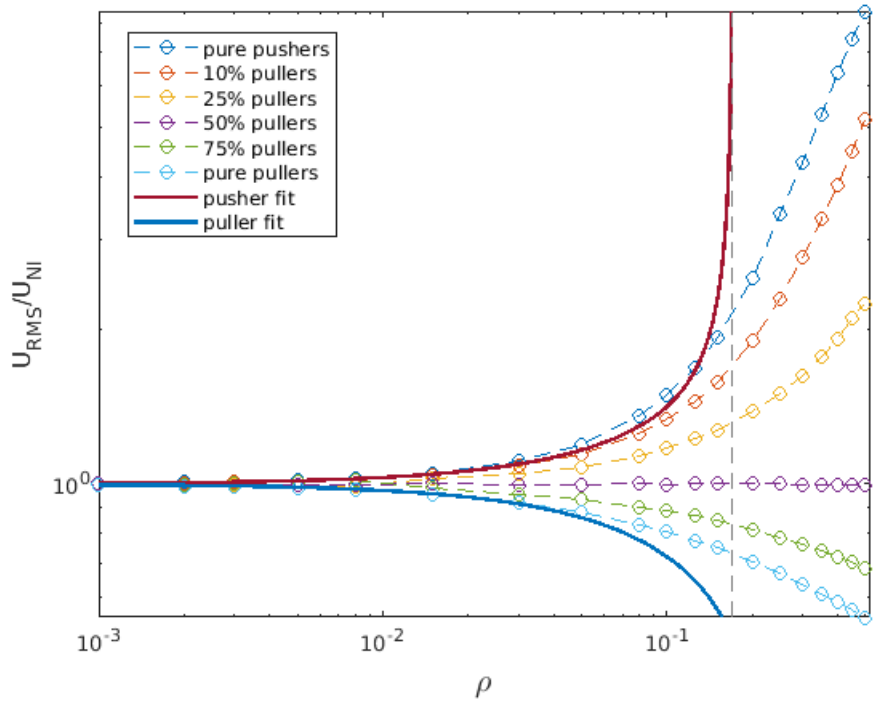

Figure 3.6: The dotted line shows U_{RMS} value normalised by the corresponding values in the non-interacting system U_{NI} for different values of X. Solid lines shows the fitted value of Eq. 3.6 to the pusher respectively puller data.

Figure 3.6 shows the normalised U_{RMS} values as a function of density. Just as in the case of the microswimmers, the U_{RMS} values for the $X = 0.5$ suspension displays the same values as the non interacting model. One difference between swimmers and shakers is the shape of the curves; the sigmodial shape of the microswimmer transition is absent in Figure 3.6. For shakers the transition is continuous and more smooth. Also notice that the values on the y-axis is smaller compared to the corresponding values for swimmers. This suggest that the effect enhances the intensity of the turbulence.

In the case of pure-pusher and-puller suspension it is known that [24] :

$$\frac{\langle \mathbf{U}^2 \rangle}{\mathbf{U}_{NI}^2} \approx \left(1 \pm \frac{\rho(2\rho_c \mp \rho)}{2\rho_c(\rho_c \mp \rho)}\right) \tag{3.6}$$

Were the upper sign corresponds to pushers and the lower sign to pullers and ρ_c is the critical density above which collective motions takes place. Eq. 3.6 was fit to the pusher and puller data, the fit was performed for $\rho < 0.1$, i.e. in the density region where we expect Eq. 3.6 to hold. A sufficiently good fit was obtained for $\rho_c \approx 0.17$. Equation 3.6 only describes small fluctuations around the homogeneous and isotropic state seen for noninteracting shakers, while higher order interactions need to be taken into account in order to properly describe the turbulent state. From these fits it is obvious that the U_{RMS} is non-additive in X, especially close to the transition density.

To characterize the flows in the fluid we proceed with studying the variation of the length and timescales, defined in accordance with chapter 4.2 (see Figure 3.3). The result is reported in Figure 3.7. The lengthscale ξ shows an apparently linear variation with ρ. The ξ values are also much smaller compared to regular swimmers, indicating much more short-ranged flows than in the corresponding swimmer suspensions. From the previous analysis we can expect that the transition to turbulence should occur around $\rho = 0.17$. However, the plots of ξ and τ versus ρ both show continuous variation with density, without any sign of such a sharp transition, in stark contrast to what we observe in the swimmer suspensions. From previous finding it is know that ρ_c should be the same for shakers and swimmers [21].

Moving on to the timescale τ, suspensions with $X \geq 0.5$ exhibit monotonic decay. In the presence of collective motion (i.e $X < 0.5$) the decay gets modified. For the pusher dominated suspension the addition of swimmers will slow down dynamics in the dilute region, while the opposite occurs in the dense region. The pure pusher suspension peaks around $\rho = 0.2$, which seems to be in approximate agreement with the estimated value of ρ_c. Over all the shakers exhibit much smaller τ values compared to swimmers. One imagines that the omission of swimming should rather act to slow down dynamics, but our results suggest the opposite.

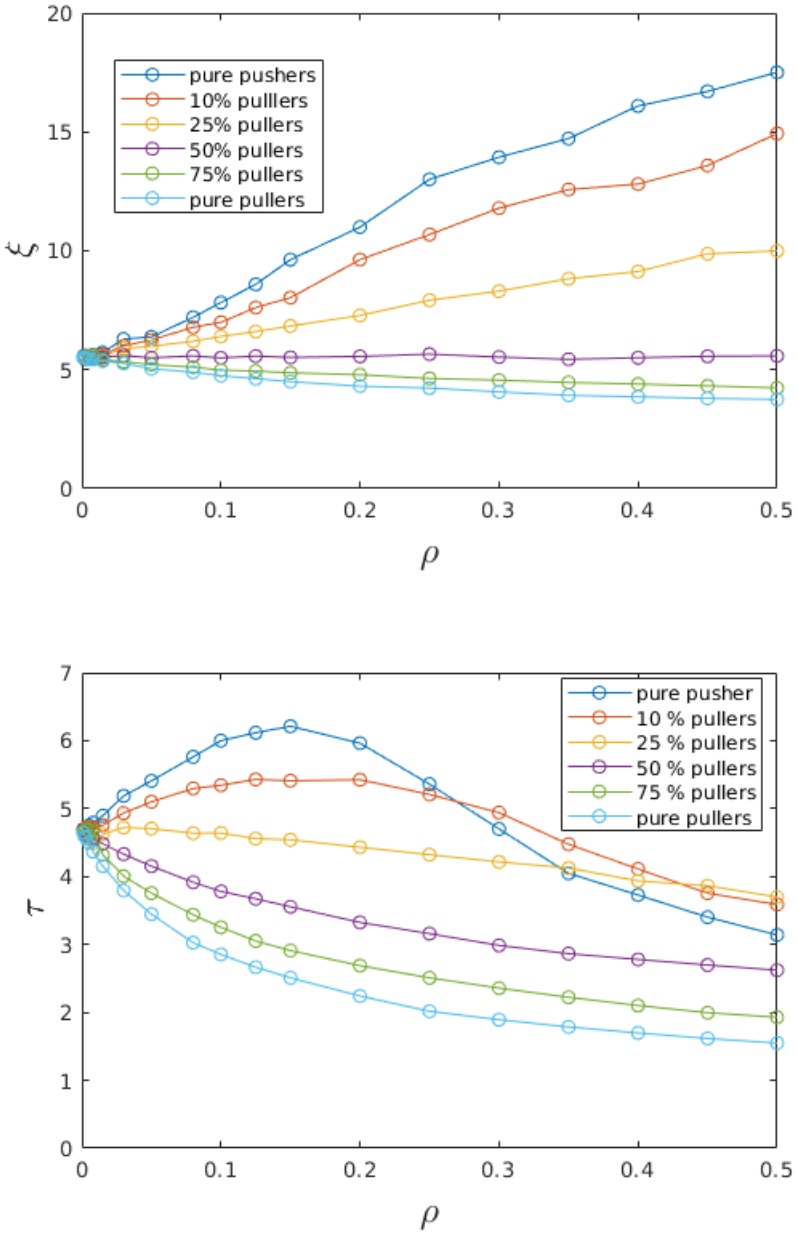

Figure 3.7: Top: The lengthscale ξ as a function of ρ for different values of X. Bottom: The timescale τ as a function of ρ for different values of X.

Conclusions and outlook

We have in this thesis investigated the properties of mixed pusher and puller suspensions. We started by studying the two body interactions. Our results show that pushers have a tendency to align whereas pullers do the opposite. In the case of the mixed pusher-puller interaction the behaviour is more complex. This is due to the fact that we no longer have action-reaction symmetry. In our studies of suspensions have seen that the addition of pullers have a tendency to inhibit collective motion. Active turbulence only occur in suspension with a majority of pushers. Addition of small amounts of pullers in a pusher suspension will effect the properties of the collective motion. Properties such a nematic ordering, transition densities and length-and timescales can be affected. We have also seen that shakers display a transition to active turbulence that is qualitatively different compared to swimmers. Our studies of shakers show that the U_{RMS} dependence up on the mixture fraction of pushers/pullers is nonadditive (in the intermediate to dens region). Our studies also suggest that systems consisting of equal part pushers and pullers will display a lot of properties that are similar to noninteracting systems.

In the simulations we made, we have made it obvious that we have neglected excluded volume interactions. It might be hard to implement an algorithm with low computational costs that accounts for this. The inclusion of nearfield hydrodynamics seems more plausible though and might be interesting to investigate for future studies. Further investigations in to the behaviour of the equal part suspension is needed as well. The question of interest here is what kind of configurations that give rise to the noninteracting behaviour. From our finding it seems as it the addition of pullers seem to shift the transition densities. More studies on this subject would be interesting as well

The results from this thesis will hopefully advance the research field of active turbulence and other areas as well. The processes were microorganisms are important are potential application area were the results might come in handy. This might for instance correspond to studies of ecological processes, prevention of biofilm build up in prosthetics or in industrial applications such as waste water treatment. It might also be relevant for applications were artificial microswimmers might find a future application. The ethical aspects surrounding the technological applications of the finding made in this thesis are quite hard to draw out.

Bibliography

[1] Richard J. Archer et al. "A Pickering Emulsion Route to Swimming Active Janus Colloids". In: *Advanced Science* 5.2 (2018), pp. 1–9. ISSN: 21983844. DOI: 10.1002/advs.201700528.

[2] Dóra Bárdfalvy et al. "Particle-resolved lattice Boltzmann simulations of 3-dimensional active turbulence". 2019. URL: https://arxiv.org/abs/1904.03069.

[3] Luis H Cisneros et al. "Fluid dynamics of self-propelled microorganisms, from individuals to concentrated populations". In: *Animal Locomotion* (2010), pp. 99–115. DOI: 10.1007/978-3-642-11633-9_10.

[4] Baohu Dai et al. "Programmable artificial phototactic microswimmer". In: *Nature Nanotechnology* 11.12 (2016), pp. 1087–1092. ISSN: 17483395. DOI: 10.1038/nnano.2016.187.

[5] Amin Doostmohammadi et al. "Active nematics". In: *Nature Communications* 9.1 (2018). ISSN: 20411723. DOI: 10.1038/s41467-018-05666-8.

[6] J. Elgeti, R. G. Winkler, and G. Gompper. "Physics of microswimmers - Single particle motion and collective behavior: A review". In: *Reports on Progress in Physics* 78.5 (2015). ISSN: 00344885. DOI: 10.1088/0034-4885/78/5/056601.

[7] Guillaume Grégoire, Hugues Chaté, and Yuhai Tu. "Comment on "particle diffusion in a quasi-two-dimensional bacterial bath"". In: *Physical Review Letters* 86.3 (2001), p. 556. ISSN: 10797114. DOI: 10.1103/PhysRevLett.86.556.

[8] Élisabeth Guazzelli and Jeffrey Morris. *A physical introduction to suspension dynamics. With illustrations by Sylvie Pic.* 2011. ISBN: 9780521193191. DOI: 10.1017/CBO9780511894671.

[9] Hong Ren Jiang, Natsuhiko Yoshinaga, and Masaki Sano. "Active motion of a Janus particle by self-thermophoresis in a defocused laser beam". In: *Physical Review Letters* 105.26 (2010), pp. 1–4. ISSN: 00319007. DOI: 10.1103/PhysRevLett.105.268302.

[10] Michael Junk and Reinhard Illner. “A new derivation of Jeffery’s equation”. In: *Journal of Mathematical Fluid Mechanics* 9.4 (2007), pp. 455–488. ISSN: 14226928. DOI: 10.1007/s00021-005-0208-0.

[11] Deepak Krishnamurthy and Ganesh Subramanian. “Collective motion in a suspension of micro-swimmers that run-and-tumble and rotary diffuse”. In: *Journal of Fluid Mechanics* 781 (2015), pp. 422–466. ISSN: 0022-1120. DOI: 10.1017/jfm.2015.473.

[12] Eric Lauga and Thomas R Powers. “The hydrodynamics of swimming microorganisms”. In: *Reports on Progress in Physics* 72.9 (2009). ISSN: 00344885. DOI: 10.1088/0034-4885/72/9/096601.

[13] R. W. Nash, R. Adhikari, and M. E. Cates. “Singular forces and point-like colloids in lattice Boltzmann hydrodynamics”. In: *Physical Review E - Statistical, Nonlinear, and Soft Matter Physics* 77.2 (2008), pp. 1–11. ISSN: 15393755. DOI: 10.1103/PhysRevE.77.026709.

[14] Giorgio Pessot, Hartmut Löwen, and Andreas M. Menzel. “Binary pusher–puller mixtures of active microswimmers and their collective behaviour”. In: *Molecular Physics* 116.21-22 (2018), pp. 3401–3408. ISSN: 13623028. DOI: 10.1080/00268976.2018.1496291. URL: https://doi.org/10.1080/00268976.2018.1496291.

[15] E. M. Purcell. “Life at low Reynolds number”. In: *American Journal of Physics* 45.1 (1977), pp. 3–11. ISSN: 0002-9505. DOI: 10.1119/1.10903. URL: http://aapt.scitation.org/doi/10.1119/1.10903.

[16] Sriram Ramaswamy. “The Mechanics and Statistics of Active Matter”. In: (2010). DOI: 10.1146/annurev-conmatphys-070909-104101. arXiv: 1004.1933. URL: http://arxiv.org/abs/1004.1933{\%}0Ahttp://dx.doi.org/10.1146/annurev-conmatphys-070909-104101.

[17] Nadeem Riaz et al. “Microbial diversity — exploration of natural ecosystems and microbiomes”. In: 118.24 (2016), pp. 6072–6078. DOI: 10.1002/cncr.27633.Percutaneous.

[18] David Saintillan. “A quantitative look into microorganism hydrodynamics”. In: *Physics* 3 (2010), p. 84. ISSN: 1943-2879. DOI: 10.1103/Physics.3.84. URL: https://link.aps.org/doi/10.1103/Physics.3.84.

[19] David Saintillan. “Emergence of coherent structures and large-scale flows in active suspensions”. In: *Slides* June (2011), pp. 9–10.

[20] David Saintillan. “Kinetic Models for Biologically Active Suspensions”. In: (2012), pp. 53–71. DOI: 10.1007/978-1-4614-3997-4_4.

[21] David Saintillan and Michael J. Shelley. “Instabilities, pattern formation, and mixing in active suspensions”. In: *Physics of Fluids* 20.12 (2008), p. 123304. ISSN: 1070-6631. DOI: 10.1063/1.3041776.

[22] Tim Sanchez et al. "Spontaneous motion in hierarchically assembled active matter". In: *Nature* 491.7424 (2012), pp. 431–434. ISSN: 00280836. DOI: 10.1038/nature11591. URL: http://dx.doi.org/10.1038/nature11591.

[23] Sparr Annika Sparr Gunnar. *Kontinuerliga system*. Studentlitteratur AB, 2001, p. 441. ISBN: 9789144013558.

[24] Joakim Stenhammar et al. "Role of Correlations in the Collective Behavior of Microswimmer Suspensions". In: *Physical Review Letters* 119.2 (2017), pp. 1–6. ISSN: 10797114. DOI: 10.1103/PhysRevLett.119.028005.

[25] Ganesh Subramanian and Donald L Koch. "Critical bacterial concentration for the onset of collective swimming". In: *Journal of Fluid Mechanics* 632 (2009), pp. 359–400. ISSN: 00221120. DOI: 10.1017/S002211200900706X.

[26] Sauro Succi, Mauro Sbragaglia, and Stefano Ubertini. "Lattice Boltzmann Method". In: *Scholarpedia* 5.5 (2010), p. 9507. ISSN: 1941-6016. DOI: 10.4249/scholarpedia.9507. URL: http://www.scholarpedia.org/article/Lattice{_}Boltzmann{_}Method.

[27] Sumesh P. Thampi, Ramin Golestanian, and Julia M. Yeomans. "Velocity correlations in an active nematic". In: *Physical Review Letters* 111.11 (2013), pp. 2–6. ISSN: 00319007. DOI: 10.1103/PhysRevLett.111.118101.

[28] Erlend Magnus Viggen Timm Krüger, Halim Kusumaatmaja, Alexandr Kuzmin, Orest Shardt, Goncalo Silva. *The Lattice Bolyzmannn Method: Principles and Practics.Pdf*. 2017. ISBN: 9783319446479. URL: http://gen.lib.rus.ec/book/index.php?md5=7B74F161BFE998821E1EB2DFF8BB336F.

[29] Patrick T. Underhill, Juan P. Hernandez-Ortiz, and Michael D. Graham. "Diffusion and spatial correlations in suspensions of swimming particles". In: *Physical Review Letters* 100.24 (2008), pp. 1–4. ISSN: 00319007. DOI: 10.1103/PhysRevLett.100.248101.

[30] J. M. Yeomans, D. O. Pushkin, and H. Shum. "An introduction to the hydrodynamics of swimming microorganisms". In: *European Physical Journal: Special Topics* 223.9 (2014), pp. 1771–1785. ISSN: 19516401. DOI: 10.1140/epjst/e2014-02225-8.